CORRELATIONS AND MEMORY IN NEURODYNAMICAL SYSTEMS

André Longtin[1], Carlo Laing[1], and Maurice J. Chacron[1]

University of Ottawa, Physics Department,
150 Louis Pasteur, Ottawa, Ont., Canada K1N 6N5

Abstract. The operation of the nervous system relies in great part on the firing activity of neurons. This activity exhibit significant fluctuations on a variety of time scales as well as a number of memory effects. We discuss examples of stochastic and memory effects that have arisen in our neuronal modeling work on a variety of systems. The time scales of these effects range from milliseconds to seconds. Qar

to formulate nonlinear dynamical equations of motion for the assumed state variables of the system must also decide on whether or not to couple stochastic forces to deterministic models.

There are certainly philosophical issues underlying these choices. For example, one can argue that the evolution of the whole dynamical system of the brain relies only on the current state of all its components. And within this purview, activity in a given cell or group of cells may display correlations b schema

"working memory" task. This memory will be either strengthened or decay away, and in any case influence the activity of the associated neurons on a long time scale. In this sense, it can be seen as a source of long range correlations. This memory will also be subjected to the effect of neuronal noise, which a priori would be considered as a limiting factor for the performance of this type of memory. We will report below on a paradoxical finding tha

a minimum as a function of the integration time. However, very little is known about how this can be generated in a biophysical neuron model.

Here we study how such a minimum can be generated in a simplified version of a model that has been used to model weakly electric fish electroreceptors [6–8]. The core of the model resides in the addition of threshold fatigue after an action potential to model refractory effects [19]. It is known that the model under Gaussian white noise stimulation gives rise to negative interspike interval (ISI) correlations that decay over short ranges [9]. We show that the addition of correlated noise gives rise to positive long range ISI correlations in the spike train generated by the model. These positive long range correlations lead to an increase in spike train variability at long time scales similar to that seen experimentally. They further interact with the short range negative ISI correlations to give rise to a minimum in spike train variability as observed experimentally. The functional consequences of both types of correlations is studied by considering their effects on the detectability of signals.

2.

Figure 1A illustrates the model dynamics. The noise sources $\xi(t)$ and $\eta(t)$ are shown in Fig. 1B. Note that we chose the noise source $\eta(t)$ to be two orders of magnitude weaker than the noise source $\xi(t)$. Also, $\xi(t)$ varies over short time scales while the noise $\eta(t)$ varies over longer time scales.

2.2 Interspike Interval Correlations

From the spike time sequence $\{t_i\}_{i=1}^{N}$, one can define the ISI sequence $\{I_i\}_{i=1}^{n} = \{t_{i+1} - t_i\}_{i=1}^{N-1}$. The ISI serial correlation coefficients (SCC) ϱ_j are a measure of linear correlations between successive ISIs. They are defined by

$$\varrho_j = \frac{< I_n I_{n+j} > - < I_n >^2}{< I_n^2 > - < I_n >^2} , \qquad (2)$$

where $< . >$ denotes an average over the ISI sequence. The SCC ϱ_j is positive if the j^{th} ISI and the current one are both (on average) shorter or longer than average. However, it is negative when the present ISI is shorter (longer) than average while the j^{th} ISI is longer (shorter) than average.

Figure 2 shows the SCC sequence obtained with the model (black curve). One observes the presence of long range weak ISI correlations that decay exponentially with increasing lag. These are due to the presence of the OU noise $\eta(t)$ [7]. The SCC sequence obtained in the absence of Ornstein-Uhlenbeck noise (i.e. $E = 0$) does not show long range correlations (gray curve). The presence of long range correlations can be explained intuitively in the following manner [7]. The noise $\eta(t)$ varies on a slower time scale than the neural dynamics: it can thus be considered quasi-constant on the average ISI time scale. Thus, if the noise $\eta(t)$ is positive, it will stay positive for a long time (see figure 1B): this will lead to a long sequence of ISIs that will be shorter than average.

Note that in both cases (i.e. with and without OU noise), we have $\varrho_1 < 0$ (see inset). This is due to the deterministhna)e 6 tidendas6 Wl iwg1 6Lida tlag; 6 6 dea t L 6 ide i g 66u
t we de 6 d) t M s t re 6 al 6 dg g 6 da f t 6 b6 da t g 6o d
g seq e scarh ere 6 (t g 6 ar gg 6, 6 by dc 6de
l e tim 6
n b 6

2.3 Detection of Weak Signals

We now discuss the use of signal detection theory [21] to assess the consequences of ISI correlations on the detectability of signals. This is based on the optimal discrimination of spike count distributions in the absence and presence of a stimulus ($P_0(n,T)$ and $P_1(n,T)$, respectively). Let us suppose that the fi

We have shown that both short range negative and long range positive ISI correlations interact to give a minimum in spike train variability at an intermediate counting time. This minimum has been observed experimentally in auditory fibers [36] as well as in weakly electric fish electroreceptors [42]. We have previously reproduced this effect using a detailed electroreceptor model [7]. However, the present study shows that similar effects can be obtained in a simple model with dynamic threshold and correlated noise. The functional consequences of this minimal counting time were assessed using signal detection theory. It was shown that the model under Gaussian white noise stimulation displayed only short range negative ISI correlations [6,9]. That result was reproduced here. It was further shown that negative ISI correlations reduced spike train variability as measured by the Fano factor at long time scales.

Using signal detection theory, we have shown that the improvement in signal detectability was maximal, as compared to a renewal process, when the Fano factor was minimal. It has been shown in weakly electric fish electroreceptors that the counting time at which the Fano factor is minimal corresponds to the behavioral time scale for prey detection [39]. Animals must make decisions in short amounts of time (usually less than a second) in order to survive (i.e. to detect prey or avoid predators). Thus, the presence of short term negative ISI correlations might serve to increase signal detectability while long term positive ISI correlations will give rise to an integration time at which spike train variability is minimal. It could be that the animal does not want to integrate the signalim

combines aspects of or

display peaks at multiples of the delay, superimposed on an overall decaying background [38]. Such structure will also be seen if noise is incorporated into the dynamical equations, leading to a "stochastic delay-differential system" (SDDE) in the latter case. Of course, the peaks will be repeated periodically, along with all the rest of the autocorrelation function, if the solution is periodic.

Usually, there is sufficient knowledge about the system under study to conclude the presence of delays. However, sometimes that fact is not clear, or the value of the delay is not known, or there could be more than one delay. There exist time series methods that allow the detection of delays, as well as estimation of these delays [25].

3.3 Delayed Neural Control

Delays arise often in the context of neural control, such as in the control of light flux on the retina in the pupil light reflex (PLR). This reflex is in fact a paradigm of neural control systems [44]. This system is interesting from an experimental point of view because it can be manipulated non-invasively using infrared video-pupillometry coupled with special light stimulation. In past work on the human pupil light reflex [33], we have been able to study the onset of oscillations as the gain of this control system is artificially increased. We have been quickly confronted with noisy fluctuations in the analysis and modeling of this system. This is not surprising given that this reflex naturally exhibits ongoing fluctuations ("hippus") in healthy humans under constant light stimulation. Such baseline fluctuations are in fact common in neural and physiological control, and their origin and meaning is a subject of great interest and debate [20]. They just happen to be especially prominent in the light

origin of this noise, its spectrum before entering the reflex arc, and its coupling to the reflex arc? Any progress along this line would be of great interest given that the pupil reflects brainstem function as well as higher brain function such as attention and wakefpe

working memory [24,29,50], among others. Working memory involves the holding and processing of information on the time scale of seconds. For these models, which involve one-dimensional arrays of neurons, the position of a bump is thought to encode some relevant aspect of the computational task. Simple versions of these models do reproduce the basic experimental aspects of short term memory [24,29].

One problem, however, is that more realistic models of the neurons involve what are known as adaptation effects. Spike frequency adaptation, in which the firing frequency of a neuron slowly declines when it is subject to a constant stimulus, is ubiquitous in cortical neurons [32]. It is known that including such adaptation in a general model for bump formation destabilizes stationary bumps, causing moving bumps to be stable instead [30]. This was shown in [30], for a particular model, to be due to a supercritical pitchfork bifurcation in bump speed as the strength of adaptation was increased. The bifurcation occurred for a non-zero value of adaptation strength. The implication of this destabilization is that, while the bump may initially be at the position that codes for the spatial stimulus, the movement of the bump will destroy this information, thus degraded the performance of the working memory.

It was also shown in [30] that adding spatiotemporal noise to a network capable of sustaining bumps effectively negated the effect of the adaptation, "restabilizing" the bump. This beneficial aspect of noise is similar in spirit to stochastic resonance [17], in which a moderate amount of noise causes a system to behave in an optimal manner. We now demonstrate this phenomenon, and later summarize its analysis.

4.2 Stochastic Working Memory

The system we study is a network of integrate and fire neurons, in which each neuron is coupled to all other neurons, but with strengths that depend on the distance between neurons. The equations for the network are

$$\frac{dV_i}{dt} = I_i - a_i - V_i + \frac{1}{N}\sum_{j,m} J_{ij}\alpha(t - t_j^m) - \sum_l \delta(t - t_i^l) \tag{13a}$$

$$\tau_a \frac{da_i}{dt} = A\sum_l \delta(t - t_i^l) - a_i \,, \tag{13b}$$

for $i = 1, \ldots, N$, where the subscript i indexes the neurons, t_j^m is the mth firing time of the jth neuron. $\delta(\cdot)$ is the Dirac delta function, used to reset the V_i and increment the a_i. The sums over m and l extend over the entire firing history of the network, and the sum over j extends over the whole network. The postsynaptic current is represented by $\alpha(t) = \beta e^{-\beta t}$ for $0 < t$ and zero otherwise. The variable a_i, representing the adaptation current, is incremented by an amount A/τ_a at each firing time of neuron i, and exponentially decays back to zero with time constant τ_a otherwise. The coupling function we use is

$$J_{ij} = 5.4\sqrt{\frac{28}{\pi}}\exp\left[-28\left(\frac{i-j}{N}\right)^2\right] - 5\sqrt{\frac{20}{\pi}}\exp\left[-20\left(\frac{i-j}{N}\right)^2\right]. \tag{14}$$

This is a "Mexican hat" type of coupling, for which nearby neurons excite one another, but more distant neurons inhibit one another. Periodic boundary conditions are used. Parameters used are $\tau_a = 5$, $\beta = 0.5$, $N = 50$, $A = 0.1$. I_i was set to 0.95 for all i, except for a brief stimulus to initiate a bump, as explained in the caption of Fig. 5. When $I_i = 0.95$ for all i, the quiescent state, $(V_i, a_i) = (0.95, 0)$ for all i, is a solution. However, it is known that with coupling of the form (14), and $A = 0$, stationary patterns of localized activity are also possible solutions [29,30].

Noise was included in (13a)-(13b) by adding or subtracting (with equal probability) current pulses of the form σe^{-t} $(0 < t)$ to each otherwise constant current I_i. The arrival times of these pulses were chosen from a Poisson distribution. The mean frequency of arrival for both positive and negative pulses was 0.1 per time unit, so the frequency for all pulses was 0.2 per time unit. The arrival times were uncorrelated between neurons. The noise intensity was varied by changing σ.

In Fig. 5 we show typical simulation results for (13a)-(13b) for two different noise levels. A spatially localized current was injected for a short period of time $(10 < t < 20)$ to move the system from the "all off" state to a bump state. This could mimic e.g. the briefly illuminated light in an oculomotor delayed response task [24,41]. We see that the activity persists after the stimulus has been removed. This is a model of the high activity seen during the "remembering" phase of a working memory task [41].

The behavior of the system for the two different values of noise is quite different: for low noise values, the bump moves with an almost constant speed. For the example in Fig. 5 (left), the bump moves to the right. This is due to the lack of symmetry in the initial conditions – it could have just as easily traveled to the left. Note that the boundary conditions are periodic. For higher noise intensities (Fig. 5, right) the bump does not have a constant instantaneous speed, rather it moves in a random fashion, often changing direction. As a result of this, the average speed during a finite-time simulation (determined by measuring how far the bump has traveled during this time interval and dividing that distance by the length of the interval) is markedly less than in the low noise case.

This is quantified in Fig. 6 where we plot the absolute value of the average speed during an interval of 200 time units (not including the transient stimulus phase) as a function of σ, averaged over eight simulations. We see that there is a critical value of σ (approximately 0.01) above which the absolute value of the velocity drops significantly – the

As mentioned, the phenomenon was also observed in a spatially-extended rate model. For a particular choice of the coupling function (the spatially continuous version of J_{ij} (14)) it was shown that the bifurcation destabilizing a stationary bump and giving rise to traveling bumps was a supercritical pitchfork bifurcation in bump speed as A increased. Motivated by this, the noisy normal form of such a bifurcation was studied and (when velocity was measured in the same way as for the spiking neuron model above) qualitatively similar slowing down was found as the noise intensity was increased.

Motivated by these results we modeled the dynamics of the noisy normal form of a supercritical pitchfork bifurcation as a persistent random walk in one dimension. The behavior of a particle undergoing such a walk is governed by the stochastic differential equation

$$\frac{dx}{dt} = I(t)\,, \tag{15}$$

where x is the position of the particle (the bump), $I(t) \in \{-v, v\}$, and the probability that $I(t)$ changes from $-v$ to v, or from v to $-v$, in time interval dt is $(\beta/2)dt$. The probability density function of x, $p(x,t)$, satisfies the telegrapher's equation:

$$\frac{\partial^2 p}{\partial t^2} + \beta \frac{\partial p}{\partial t} = v^2 \frac{\partial^2 p}{\partial x^2}\,. \tag{16}$$

This equation can be explicitly solved, and the mean absolute position at time t, and the variance of this quantity, can both be found analytically [30]. The

22. S. Guillouzic, I. L'Heur

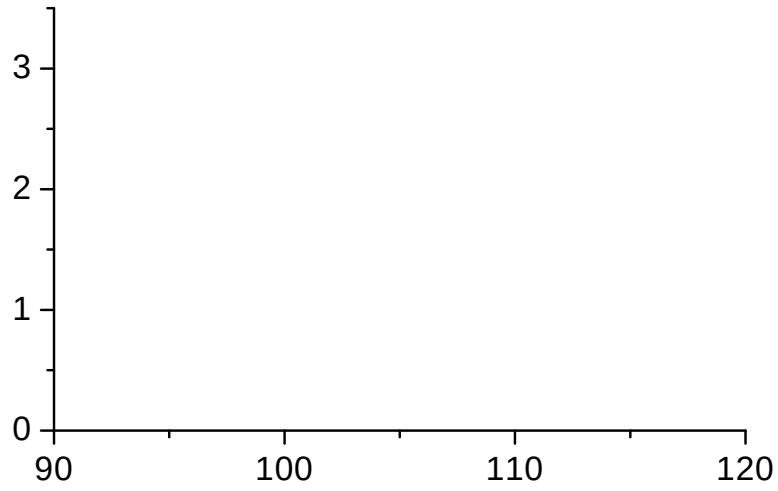
3
2
1
0
90
100
110
120

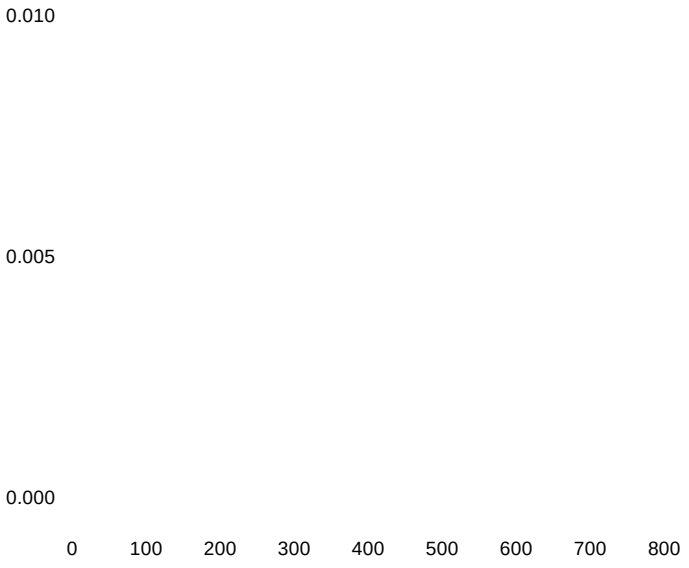
0.010
0.005
0.000
0
100
200
300
400
500
600
700
800

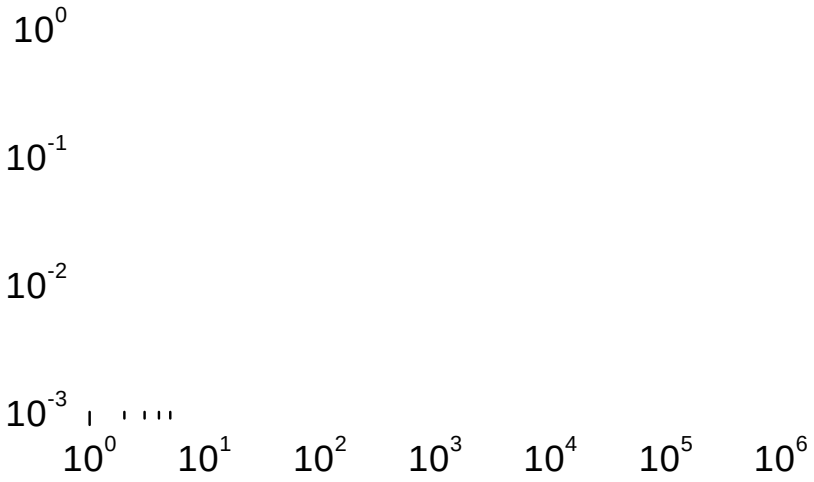
10^{0}
10^{-1}
10^{-2}
10^{-3}
10^{0}
10^{1}
10^{2}
10^{3}
10^{4}
10^{5}
10^{6}

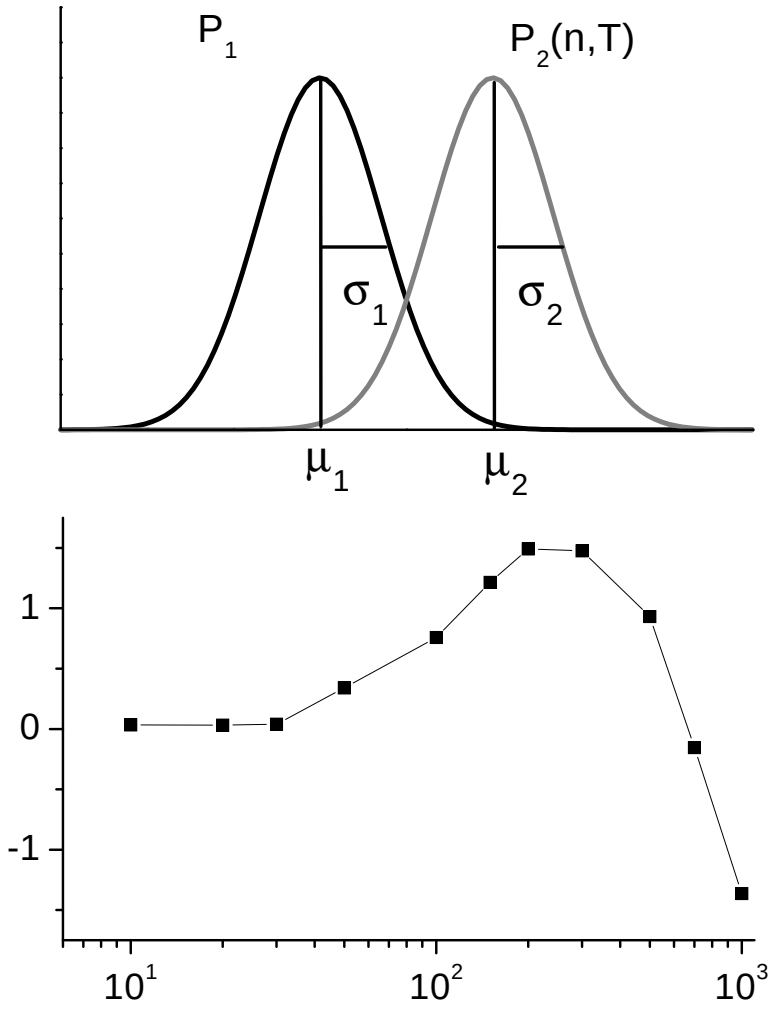
P1
P2(n,T)
σ1
σ2
μ1
μ2
1
0
-1
10^1
10^2
10^3

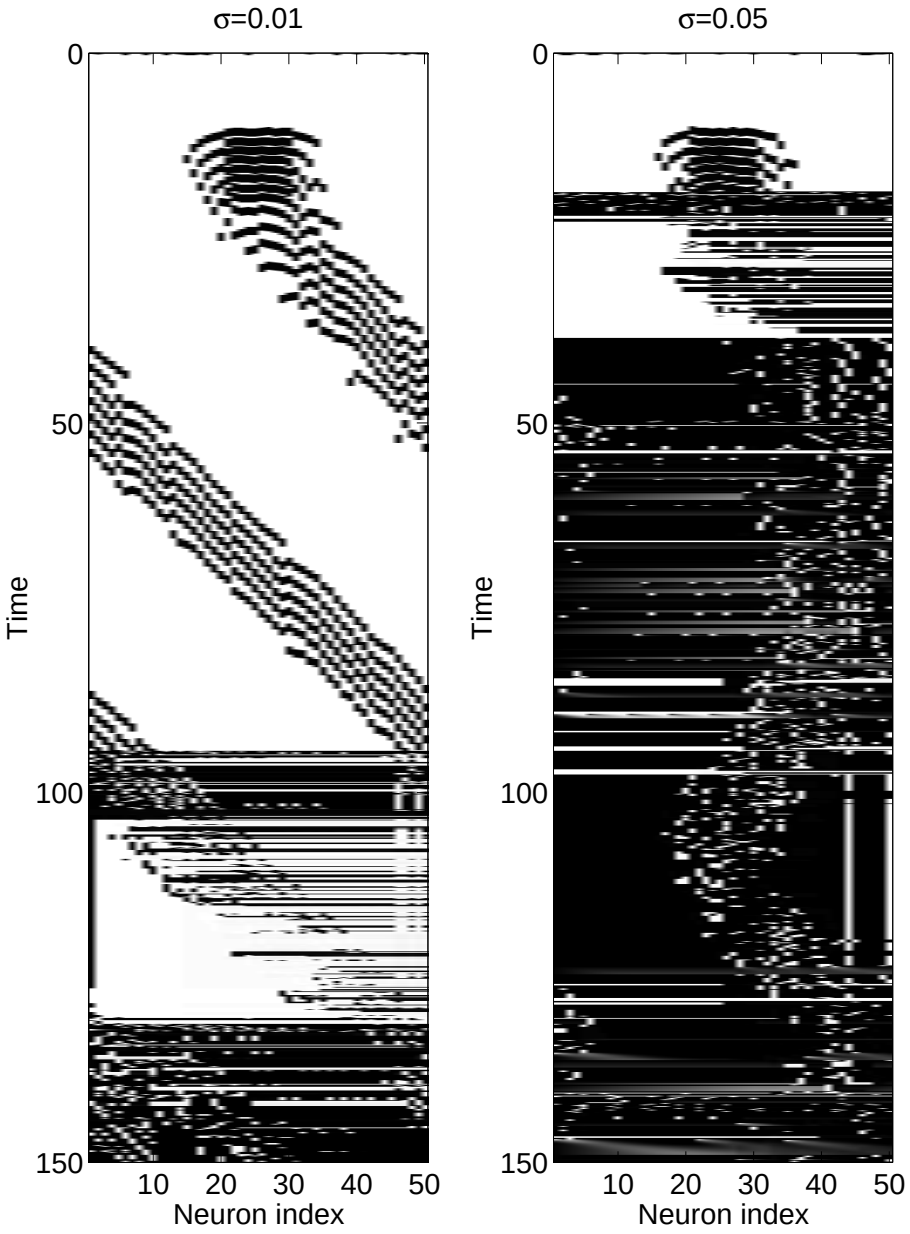

Fig. 5. Typical simulations of (13a)-(13b). (**Left**) $\sigma = 0.01$, (**Right**) $\sigma = 0.05$. A black bar is plotted each time a neuron fires (n fi

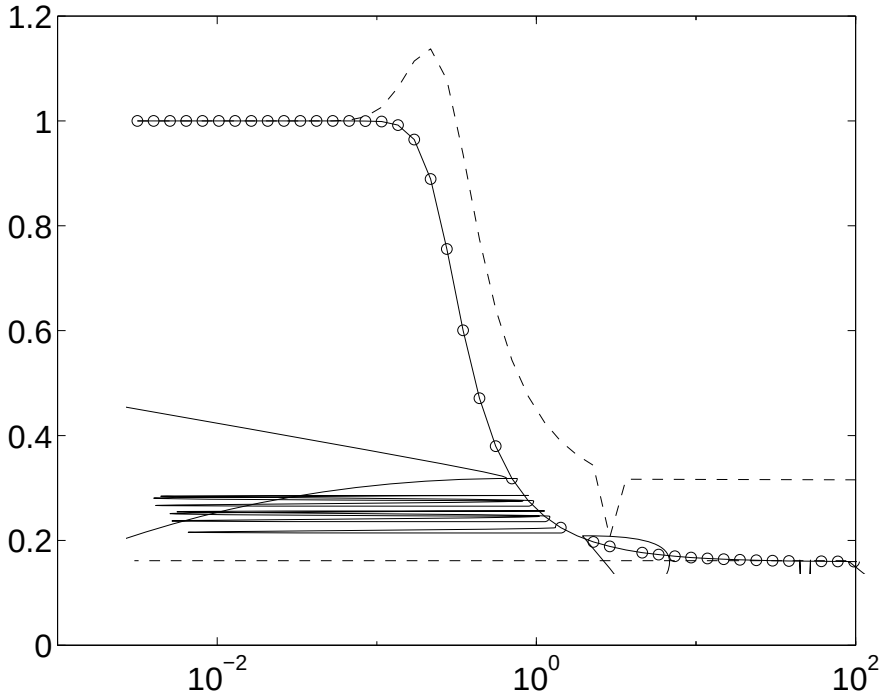
1.2
1
0.8
0.6
0.4
0.2
0
10^{-2}
10^{0}
10^{2}